Article

Controlled Synthesis of Supported Nickel Boride Catalyst Using Electroless Plating

Zhi-Jie Wu, Shao-Hui Ge, Ming-Hui Zhang, Wei Li, Shi-Cheng Mu, and Ke-Yi Tao

J. Phys. Chem. C, **2007**, 111 (24), 8587-8593• DOI: 10.1021/jp070096k • Publication Date (Web): 27 May 2007

Controlled Synthesis of Supported Nickel Boride Catalyst Using Electroless Plating

Zhi-Jie Wu,[†] Shao-Hui Ge,[†] Ming-Hui Zhang,*[,†] Wei Li,[†] Shi-Cheng Mu,[‡] and Ke-Yi Tao[†]

Institute of New Catalytic Materials Science, College of Chemistry, Nankai University, Tianjin 300071, People's Republic of China, and China National Academy of Nanotechnology and Engineering, Tianjin 300457, People's Republic of China

Received: January 5, 2007; In Final Form: February 28, 2007

The supported nickel boride (Ni−B/MgO) catalysts have been synthesized using electroless plating method. The effects of reaction parameters including the molar ratios of the starting materials, pH value of the plating solution, and the additives have been systematically studied. The catalysts have been characterized by various techniques such as inductively coupled plasma atomic emission spectrometry, high-resolution transmission electron microscopy, scanning electron microscopy, and chemisorption of hydrogen. The hydrogenating properties were evaluated using the liquid-phase hydrogenation of sulfolene and acetophenone. We found that (1) the size, compositions, and load of porous Ni−B nanoparticles depended on the starting ratio of ethylenediamine/Ni^{2+} and pH value; (2) the addition of stabilizer to plating solution resulted in changing from a porous Ni−B particle to a solid one, (3) the surface properties of supported Ni−B catalysts depended on their sizes, loading, and compositions, and (4) the hydrogenation activity depended on the surface concentrations of nickel.

1. Introduction

The development of novel materials is a fundamental point of chemical research, which has been promoted by progress in nanotechnology.[1] Investigations of heterogeneous catalytic reactions have led to an increasing development of a new type of metal boride catalysts.[2] Because of their refractory nature, resistances to sulfur poisoning, and desulphurization ability in organic synthesis, metal borides have been considered as potentially desirable catalysts.[3] The synthesis of metal borides, such as iron boride, cobalt boride, and nickel boride, has been studied in detail.[4] Among them, nickel boride (Ni−B) was shown in amorphous structure and found to be a superior hydrogenation catalyst.[5] In particular, the unsupported Ni−B catalysts have shown excellent activity in various hydrogenation reactions.[6] Therefore, the preparation and properties of unsupported Ni−B catalyst have been investigated frequently.[7]

On the other hand, the supported metal catalysts were developed for the stability and economy in preparation. For these catalysts, the catalytic activity of the metal particles is strongly influenced by their sizes and shape.[8,9] The most promising way to prepare metal clusters of uniform size and shapes on a support certainly is the deposition of mass-selected clusters from gas phase.[10] However, it is often difficult to control the morphology of the active metal on support, notably for catalysts prepared from impregnation.[8,11] Generally, the supported Ni−B catalysts are often prepared by impregnation−reduction method. Chen has reported the preparation of mesoporous silica-supported amorphous Ni−B catalysts for the selective hydrogenation of 2-ethylanthraquinone.[12] The results show that the particles sizes and dispersion of Ni−B particles vary for different supports. Recently, the sizes and compositions controls of unsupported nickel phosphide (Ni−P) particles have been carried out by chemical reduction.[13] Other than different particles sizes were obtained, most of the Ni−B or Ni−P particles prepared by the chemical reduction all were presented as solid spheres on support. The preparation of supported catalysts from metal colloids could be an alternative method to make supported catalysts with well-defined metal particles including core−shell, network, or porous structures.[14] However, the preparation of supported Ni−B catalyst is difficult because there is only weak interaction between metal colloids and the support.[15] Meanwhile, the method for improving the weak interaction is restricted by the unstable structure of amorphous alloy.

Besides the synthesis of amorphous Ni−B catalysts from the chemical reduction method, the amorphous Ni−B film or hollow spheres catalysts have been synthesized by electroless nickel (EN) plating.[16] Here, we indicate that the shapes and sizes of metal or alloy particles on substrate can be controlled by electroless plating.[17,18] The EN plating is characterized by the autocatalytic deposition of nickel, which occurs selectively in certain areas with appropriate surface condition.[16] Typically, the constituents of an EN-plating solution include a source of nickel ions, a reducing agent, suitable complexing agents, and stabilizers/inhibitors, etc. Previously, we have shown that the porous Ni−B particles can be prepared by a silver-catalyzed EN-plating technique.[19] In this work, we will investigate the effects of the molar ratio of complexing agents/Ni^{2+}, pH value, and the presence of stabilizer on the properties of nanosized Ni−B particles. We demonstrate that the control of size, shape, and load of Ni−B nanoparticles is feasible. Furthermore, the as-prepared catalysts were tested by the liquid-phase hydrogenation of sulfolene and acetophenone (AP).

2. Experimental Details

2.1. Preparation of Samples. Nickel(II) sulfate hexahydrate ($NiSO_4 \cdot 6H_2O$), potassium borohydride (KBH_4), ethylenediamine ($H_2NCH_2CH_2NH_2$), sodium hydroxide (NaOH), silver nitrite ($AgNO_3$), and lead sulfate ($PbSO_4 \cdot 2H_2O$) were of reagent grade

* Corresponding author. E-mail: zhangmh@nankai.edu.cn. Tel.: +86-22-23507730. Fax: +86-22-23507730.
[†] Nankai University.
[‡] China National Academy of Nanotechnology and Engineering.

10.1021/jp070096k CCC: $37.00
Published on Web 05/27/2007

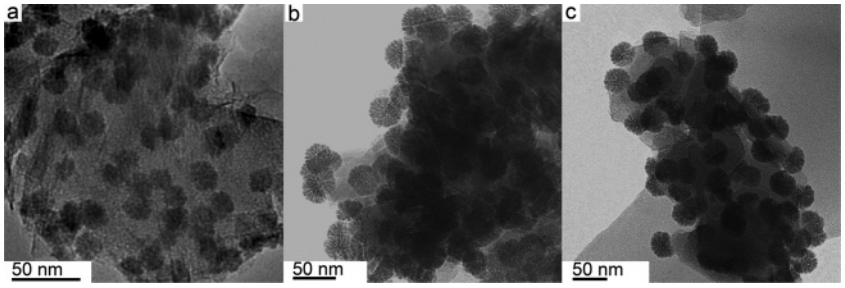

Figure 1. TEM images of series-supported amorphous Ni−B_{3-y} catalysts, prepared using a different pH value, with particle sizes of (a) Ni−$B_{3-12.8}$, 16 ± 1.2 nm, (b) Ni−$B_{3-13.2}$, 33 ± 1.5 nm, and (c) Ni−$B_{3-13.6}$, 36 ± 1.4 nm.

and were used as received. MgO support was pretreated at 773 K for 4.0 h. The Ag/MgO was synthesized as reference,[19,20] and the load of silver on support was controlled at 0.2 wt %. The plating solution consisted of nickel(II) sulfate hexahydrate (9 g L^{-1}), ethylenediamine (4∼24 g L^{-1}), and potassium borohydride (3.75 g L^{-1}). The pH value was adjusted by sodium hydroxide. To prepare the supported amorphous Ni−B/MgO catalyst, the Ag/MgO precursor was added into 200 mL of as-prepared plating solution with stirring at 323 K. The reaction lasted 20∼40 min until no significant bubbles were observed. The pH value of the plating solution varied slightly during the electroless plating (within 0.2). The resulting Ni−B/MgO was filtered and was washed thoroughly with deionized water until the pH value reached 7, then was washed with ethanol. The samples were soaked in absolute ethanol before characterization and hydrogenation. Five series of supported Ni−B samples were prepared by adjusting the molar ratio of ethylenediamine (en)/Ni^{2+} and the pH value in the above procedure and were designated as Ni−B_{x-y}, respectively, with *x* denoting the values of the nominal ratio of complexing agents/Ni^{2+} (en/Ni^{2+}) and *y* for the pH value. The plating was carried out in Carousel 6 Place Reaction Station (Radleys, UK). The variation of temperature at plating was less then 1 K from the set point. Deionized water from a Millipore Milli-Q system having a resistivity greater than 18.2 MΩ·cm was used in the sample preparations. The nickel sulfate concentration in the plating solution was calculated to obtain the catalyst with load of 10∼15 wt % nickel.

2.2. Characterization. The chemical compositions of the samples were analyzed by inductively coupled plasma atomic emission spectrometry (ICP-AES) on an IRIS Intrepid spectrometer. Transmission electron microscopy (TEM) images were acquired using a JEOL-2010 FEF high-resolution transmission electron microscope equipped with an EDX system (EDAX) and a Philips Tecnai G^2 high-resolution transmission electron microscope. The average size and size distribution of each specimen were evaluated from ∼200 randomly selected particles. The surface morphology and the diffusion of Ni−B particles on supports were observed by the scanning electronic microscopy (SEM) performed on a LEO 1530VP instrument. The differential scanning calorimetry (DSC) curves of catalysts were carried out on a Mettler Toledo DSC823e, with 40 mL/min nitrogen flow and a heating rate of 10 K/min.

The active surface area (S_{Ni}) was determined by the hydrogen chemisorption, which was performed by using a dynamic pulse method.[21] The catalyst was purged by a N_2 stream (purity of 99.999%) for 1.0 h at 473 K, which was well below its crystallization temperature. Then, the sample was cooled to room temperature, hydrogen pulses were injected at 303 K until the calculated areas of consecutive pulses were constant. In accordance to the hydrogen chemisorption, S_{Ni} and the number of surface Ni atoms were calculated assuming H/Ni(s) = 1 and a surface area of 6.5×10^{-20} m^2 per Ni atom, based on an average of the areas for the (100), (110), and (111) planes.[21]

2.3. Activity Testing. The catalytic experiments were carried out on a 100 mL stainless steel autoclave. The stirring effect was preliminarily investigated and a stirring rate of 800 rpm was employed, which turned out to be sufficient to eliminate the diffusion limit. In accordance to the hydrogen consumption recorded from a mass flow controller, the hydrogen uptake rates (i.e., the hydrogen consumption per min) were calculated according to the ideal gas equation. In the hydrogenation of sulfolene, 1.0 g catalyst (dried at 353 K with 40 mL/min 99.9% N_2 flow) was transferred into the solution composed of 30.0 mL deionized water and 30.0 g sulfolene. After replacing the air with H_2 in the reactor, the reaction was performed at 328 K and 2.0 MPa of H_2 pressure for 100 min. For AP hydrogenation, 0.6 g of dry catalyst (treated as above), 5.0 g of AP, and 60.0 mL of ethanol were mixed, then were carried out at 1.0 MPa H_2 pressure, 373 K for 4.0 h. The hydrogenation product was filtered to remove the solid catalyst and was analyzed by a gas chromatograph equipped with a flame ionization detector.

3. Results and Discussion

Our previous results showed that the catalytic properties of the supported amorphous nickel boride catalysts from silver-catalyzed EN depended on the nature of nickel boride particles on support, such as the S_{Ni} value, distribution of Ni−B particles and load of Ni−B particles.[19] It was found that the S_{Ni} value of Ni−B/MgO is higher than that of Ni−B/TiO_2. Furthermore, the effects of the amount of KBH_4 and silver in the plating solution and plating temperature have been studied. In the present study, we report the results obtained over supported Ni−B/MgO catalysts with various preparation conditions.

3.1. Synthesis of Supported Ni−B/MgO Catalyst. *A. Effects of the Complexing Agents/Ni^{2+} Molar Ratio and pH Value.* The plating solution was prepared at the molar ratios of en/Ni^{2+} ions less than 2. The complex of Ni^{2+} and en will be reduced by KBH_4 immediately during the process of preparing plating solution. However, the addition of sodium hydroxide to plating solution with en/Ni^{2+} = 2 resulted the depositions of $Ni(OH)_2$ immediately, which prevented the reduction of potassium borohydride as well. When the value of en/Ni^{2+} was higher than 2.5, the depositions of $Ni(OH)_2$ was avoided without the influence of NaOH. Thus, the nominal molar ratio of en/Ni^{2+} = 2 was discussed respectively and the other ratios were selected at 3, 4, 6, and 8. The pH value was changed from 12.4 to 13.6. The corresponding products were designated as Ni−$B_{3-12.4}$, Ni−$B_{3-13.6}$, Ni−$B_{4-12.4}$, Ni−$B_{6-12.4}$, etc. Other conditions were fixed at a KBH_4/Ni^{2+} molar ratio of 2.0 and a plating temperature of 323 K. [19b]

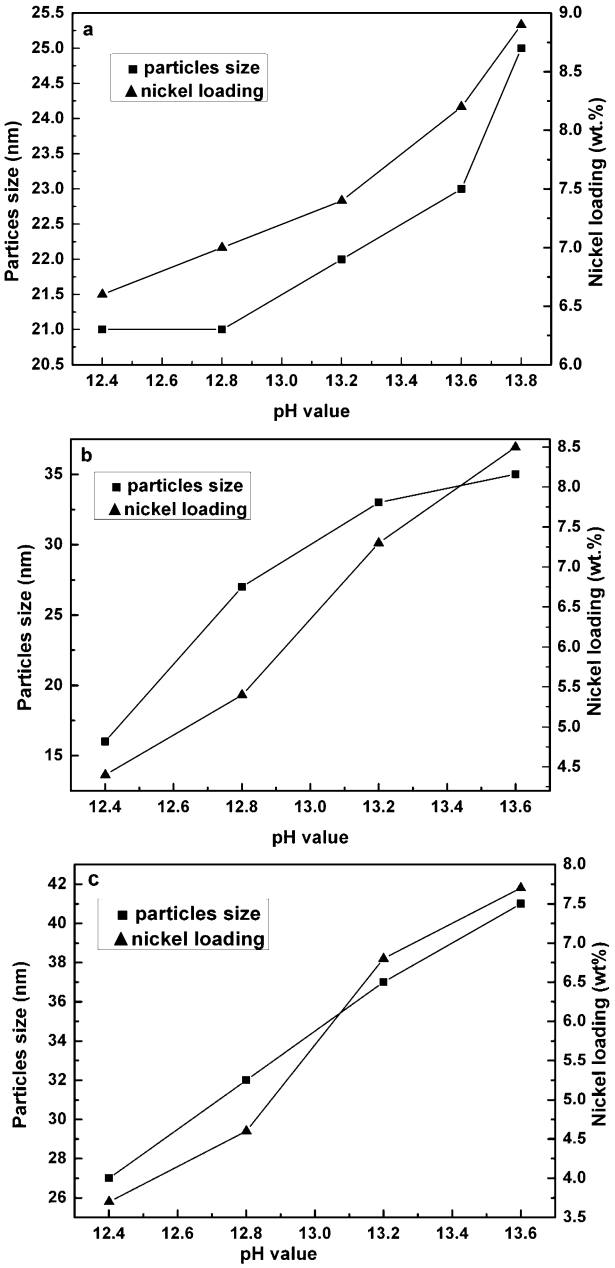

Figure 2. Particle sizes and load of nickel of the Ni−B nanoparticles plotted as a function of pH value. (a) Ni−B_{2-y} series-supported Ni−B/MgO catalysts, (b) Ni−B_{3-y} series-supported Ni−B/MgO catalysts, and (c) Ni−B_{4-y} series-supported Ni−B/MgO catalysts.

SCHEME 1: Reaction of Ni^{2+} with BH^4- in Electroless Plating

$$2BH_4^- + 4Ni^{2+} + 8OH^- \longrightarrow 4Ni + 2BO_2^- + 4H_2O \quad (1)$$

$$2BH_4^- + 4Ni^{2+} + 6OH^- \longrightarrow 2Ni_2B + 6H_2O + H_2 \quad (2)$$

Figure 1 shows the photographs of Ni−B_{3-y} (en/Ni^{2+} = 3 at different pH value) samples. The porous structures of Ni−B particles show distinctly at a higher pH value. With the increment of pH value, the average particle size increases monotonically from ~16 to ~35 nm. Moreover, the particles in each sample are uniform in size and exhibit a narrow size distribution, which is in agreement with the ref 19a. Figure 2 shows the effect of pH value on the load and sizes of Ni−B particles over different Ni−B_{x-y} series.[5] Beside Ni−B_{3-y} catalyst, the other two types of Ni−B/MgO also show the increasing of particles sizes and nickel loading with pH value. The growth of particle size is the result of gradual increased

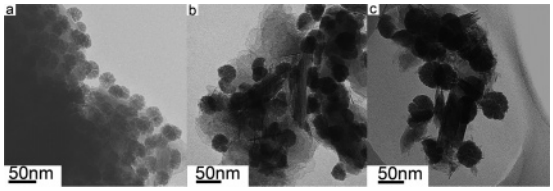

Figure 3. TEM images of supported amorphous Ni−B catalysts, prepared using different en/Ni^{2+} with the same pH value, with particle sizes of (a) Ni−$B_{2-13.6}$, 25 ± 1.1 nm, (b) Ni−$B_{4-13.6}$, 41 ± 1.4 nm, and (c) Ni−$B_{8-13.6}$, 50 ± 1.4 nm.

TABLE 1: The Compositions of Supported Amorphous Ni−B_{x-y} Catalysts

samples	plating time (min)	compositions (at %)	S_{Ni} (m^2/g)
Ni−$B_{2-12.6}$	18	$Ni_{60.8}B_{39.0}$	1.2
Ni−$B_{2-12.8}$	17	$Ni_{61.0}B_{39.0}$	1.4
Ni−$B_{2-13.2}$	14	$Ni_{61.0}B_{39.0}$	1.6
Ni−$B_{2-13.6}$	12	$Ni_{61.1}B_{38.9}$	1.8
Ni−$B_{3-12.4}$	27	$Ni_{68.9}B_{31.1}$	1.1
Ni−$B_{3-12.8}$	25	$Ni_{69.5}B_{30.5}$	1.5
Ni−$B_{3-13.2}$	20	$Ni_{70.9}B_{29.1}$	1.7
Ni−$B_{3-13.6}$	19	$Ni_{72.6}B_{27.4}$	1.8
Ni−$B_{4-12.4}$	31	$Ni_{71.8}B_{29.2}$	1.0
Ni−$B_{4-12.8}$	27	$Ni_{72.0}B_{28.0}$	1.3
Ni−$B_{4-13.2}$	22	$Ni_{73.5}B_{26.5}$	1.6
Ni−$B_{4-13.6}$	21	$Ni_{75.4}B_{24.6}$	1.7

nickel loading. For the plating solution, the complexing agents performing in the electroless plating bath are used to reduce the concentration of free nickel ions.[18] Generally, nickel ions in aqueous solution interact with and are bound to a specific number of water molecules, $[Ni(H_2O)_x]^{2+}$ ($x = 1-6$). And more aqueous nickel ions (or $[Ni(H_2O)_x]^{2+}$ ($x = 1-6$)) in the plating solution lead to a more positive electrochemical potential of Ni^{2+}.[18,22] In the plating solution, the water molecules coordinated to the nickel are replaced by en to form $[Ni(en)]^{2+}$, $[Ni(en)_2]^{2+}$, and $[Ni(en)_3]^{2+}$, which reduces the concentration of $[Ni(H_2O)_x]^{2+}$ ions. So, the higher en/Ni^{2+} molar ratio was, the more negative electrochemical potential of Ni^{2+} was obtained. Thus, different nickel loading on the Ni−B/MgO catalyst was found at different initial en/Ni^{2+} values although with the same pH value. In comparison with different initial en/Ni^{2+}, the load of nickel changes slightly with pH value for the lowest initial en/Ni^{2+} molar ratio (Figure 2a). The growth of Ni−B particles is the result of the continuous depositions of Ni−B clusters on the active surface of Ni−B particles in the electroless-plating process. [18c] In this work, we found that the load and particles sizes of Ni−B particles should be controlled simultaneously by the changes of the molar ratios of en/Ni^{2+} and pH value.

The ICP results indicated that the compositions of Ni−B particles related with en/Ni^{2+} ratios and pH value (Table 1). As a comparison, the compositions of Ni−B_{2-y} series change little. For the Ni−B_{3-y} and Ni−B_{4-y} series, the more en/Ni^{2+} ratio and higher pH value lead to a larger amount of nickel in Ni−B particles. As far as the complex of nickel ions and en are concerned, the increase in the pH value results in a decrease in the concentration of the metal ion,[17,23] but the load of nickel increases with the pH value. The possible reaction of Ni^{2+} by BH_4^- is shown in Scheme 1.[24]

With the increase of pH value, the concentration of the OH^- ions rises and the equilibrium of reaction (1) and (2) tends to the right, which resulted in depositing more Ni or Ni_2B clusters on the support and then promoting the load of Ni−B particles. As shown in Figures 1 and 2b, a higher load of nickel leads to the growth of Ni−B particles. Furthermore, higher concentrations of OH^- ions drive the occurrence of reaction (1), which

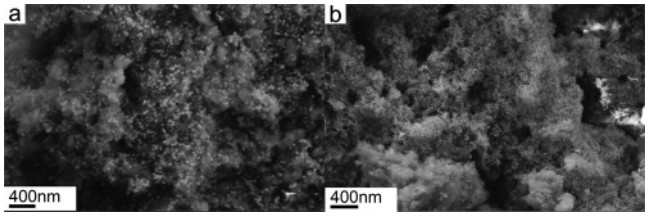

Figure 4. SEM images of the specimens (a) Ni−$B_{3-13.6}$, with 8.5 wt % nickel loading and (b) Ni−$B_{3-13.6}$, with 15.5 wt % nickel loading.

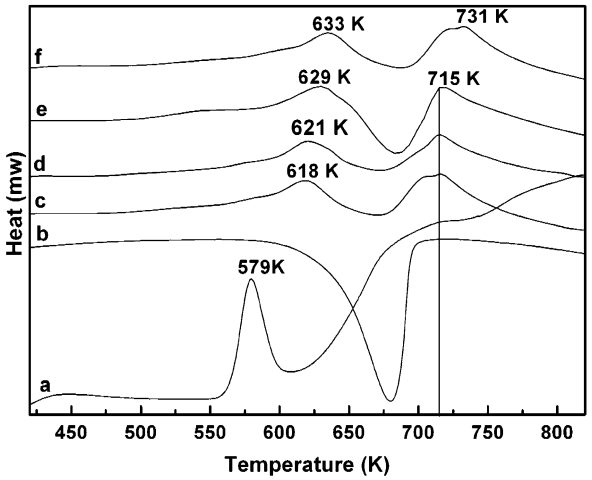

Figure 5. DSC curves of the specimens (a) unsupported Ni−$B_{3-13.6}$, (b) Ag/MgO support, (c) Ni−$B_{2-13.6}$ with 8.2 wt % nickel loading, (d) Ni−$B_{3-13.6}$ with 15.5 wt % nickel loading, (e) Ni−$B_{3-13.6}$ with 8.5 wt % nickel loading, and (f) Ni−$B_{4-13.6}$ with 7.7 wt % nickel loading.

means that the deposition of clusters is mostly due to Ni clusters other than Ni_2B clusters. Therefore, the content of nickel in Ni−B particles increases with the increase of pH value. On the other hand, the load of nickel decreases at the same pH value with the increase of the en/Ni^{2+} molar ratios according to the reactions of (1) and (2). As the concentration of nickel ions is reduced with more en in the plating solution, it should be anticipated that the higher en/Ni^{2+} ratios result in smaller Ni−B particle sizes. However, Figure 3 indicates that the Ni−B particles turn to grow at higher en/Ni^{2+} molar ratios. In general, there are four principal functions that complexing agents in the traditional EN plating bath: preventing the pH of the solution from decreasing too fast, preventing the precipitation of nickel salts, reducing the concentration of free nickel ions, and affecting the deposition reaction. However, the effect of complexing agents on the deposition reaction is not clear.[25] Most people concentrated on the plating rate affected by complexing agents, and different agents showed reversed promotion effect. It has been reported the complexing agents absorbed on the active metal improve the catalytic Ni^{2+} reduction and clusters deposition in many EN-plating processes.[24] In our experiments, the growth of Ni−B particles may be due to the superfluous en absorbed over the active metal surface.

We have studied the effect of the en/Ni^{2+} molar ratio and pH value. The nickel loading, the particles size and composition of Ni−B particles can be controlled by adjusting pH value at a certain en/Ni^{2+}. Alternatively, the particles sizes can be adjusted by changing the en/Ni^{2+} at same pH value. In addition, we have tried to make the supported Ni−B sample with the similar particles sizes while different load of nickel at the same en/Ni^{2+} and pH value. For the silver-catalyzed EN plating technique, the Ni−B particles are distributed homogeneously over the support, and the nickel or boron tends to deposit on the defects of surface, such as pores, pits, and cracks, because

TABLE 2: The Compositions of Supported Amorphous Ni−$B_{3-13.6}$ Catalysts

samples[a]	plating time (min)	Pb^{2+} (ppm)	nickel loading (wt %)	S_{Ni} (m^2/g)	compositions (at %)
Ni−$B_{3-13.6}$	19	0	8.5	1.8	$Ni_{72.6}B_{27.4}$
Ni−$B_{3-13.6-1}$	42	10	5.1	1.2	$Ni_{78.7}B_{21.3}$
Ni−$B_{3-13.6-2}$	97	50	3.8	1.0	$Ni_{80.2}B_{19.8}$
Ni−$B_{3-13.6-3}$	216	100	3.1	0.8	$Ni_{81.3}B_{18.7}$

[a] The EN plating was carried out at the same condition as the supported Ni−$B_{3-13.6}$ catalyst.

of the high surface energy.[21,26] After the dispersion of nickel nuclei over the support, the BH_4^- are absorbed on the surface of the Ni or Ni−B nuclei, forming an electrical double-layer. As the nature of the layer between support and plating varies with different pH values and supports, the growth of Ni−B particles changed with the pH value. Meanwhile, the Coulombic repulsion will reduce the rate of further particle aggregation.[13,22] Therefore, when the amount of support (Ag/MgO) was reduced from 3.6 to 1.6 g (controlling the numerical load of nickel at 20 wt %) during the electroless-plating of Ni−$B_{3-13.6}$, the particle sizes (determined by TEM images) of Ni−B nanoparticles stayed the same while higher density Ni−B particles were over MgO (Figure 4). For the supported nickel catalyst from impregnation−reduction, higher nickel loading results in increasing particles size of nickel crystalline and decreasing the S_{Ni} value.[27,28] In contrast, the EN route for supported Ni−B catalyst preparation is immune to such problems. The results suggest that the Ni−B particles were formed by the aggregation of Ni−B clusters, and the sizes of aggregation depend on the pH value and concentration of reagents.[1]

Figure 4 suggests that the fixed pH value and concentration of reagents result in the constant particles size of Ni−B particles. Because the dispersion of Ni−B particles depends on the surface sites with defects, such as pores, pits, and cracks, it can be anticipated that superfluous Ni−B particles are inevitable absorbed by support without strong interaction of Ni−B particles when the nickel loading increases sharply. Figure 5 shows the differential scanning calorimetry (DSC) curves of unsupported and supported Ni−B catalysts. The curve of Ag/MgO with temperature shows that the support absorbs additional energy during heat treatment. The crystallization temperature of unsupported Ni−$B_{3-13.6}$ is at 579 K, while a higher temperature between 618 and 633 K is obtained when the support is introduced. The increase of crystallization temperature is due to the strong interaction of support and Ni−B particles.[6] A higher en/Ni^{2+} molar ratio are in favor of higher crystallization temperature, as shown in Figure 5c,e,f. For Ni−$B_{3-13.6}$ catalysts, when the nickel loading increases from 8.5 to 15.5 wt %, the crystallization temperature decreases 8 K. It could be due to the exothermic reaction from which the sample with higher nickel loading releases more heat.[29,30] The result shows that the strong interaction between Ni−B particles and support occurs on supported Ni−$B_{3-13.6}$ catalyst with 8.5∼15.5 wt % load of nickel.

B. Effect of Stabilizer. The particle size and load of Ni−B particles can be controlled by adjusting reaction conditions, such as en/Ni^{2+}, pH value, and the amount of support used in an EN plating process. Yin et al. found that the lead ions inhibit the propagation of nickel particles through displacement reaction with nickel atoms.[18b] They pointed out that the Pb^{2+} ions act by lowering the reductive potential of the plating frontier after Pb atoms are codeposited into the Ni lattice. Alternatively, the Pb atoms play a catalytic role in the deactivation of Ni particles and then reduce the amount of hydrogen atoms formed on the

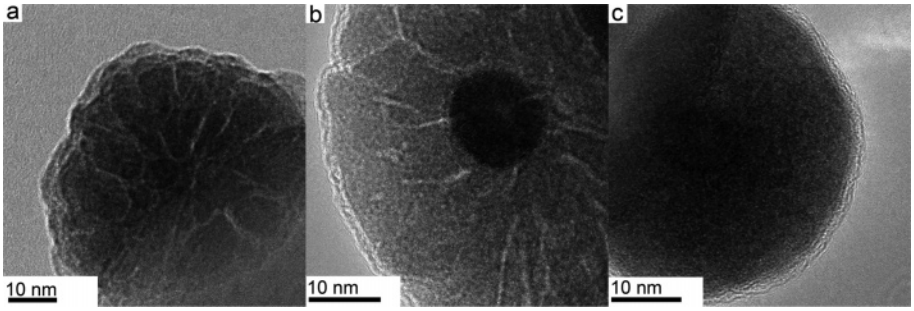

Figure 6. HRTEM images of supported Ni−B catalysts. (a) Ni−$B_{3-13.6}$; (b) Ni−$B_{3-13.6}$-2(Pb); and (c)Ni−$B_{3-13.6}$-2(Pb).

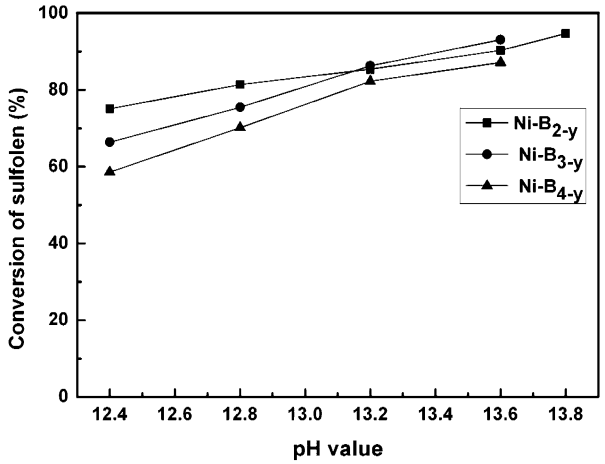

Figure 7. Catalytic activity plotted as a function of pH value. (1) Ni−B_{2-y} series−supported Ni−B/MgO catalysts, (2) Ni−B_{3-y} series-supported Ni−B/MgO catalysts, and (3) Ni−B_{4-y} series-supported Ni−B/MgO catalysts. The amount of catalyst in hydrogenation of sulfolene is 0.5 g.

TABLE 3: The Compositions of Supported Amorphous Ni−B Catalysts and Catalytic Activities in Sulfolene Hydrogenation

samples	nickel loading (wt %)	S_{Ni} (m^2/g)	compositions (at %)	conversion (%)
Ni-$B_{2-13.6}$	9.4	1.9	$Ni_{62.0}B_{38.0}$	99.9
Ni-$B_{3-13.6}$	9.8	1.9	$Ni_{72.8}B_{27.2}$	99.8
Ni-$B_{4-13.6}$	9.8	1.8	$Ni_{75.2}B_{24.8}$	98.1
Ni-$B_{6-13.6}$	10.1	1.5	$Ni_{76.8}B_{23.2}$	77.6
Ni-$B_{8-13.6}$	9.9	1.1	$Ni_{77.4}B_{22.6}$	56.4

active Ni surface. Thus, it can be anticipated that the porous structure from the emission of hydrogen during EN plating should disappear. Table 2 shows the influence of Pb^{2+} for the supported amorphous Ni−B catalysts. With the increase of Pb^{2+} concentration in the plating solution, the plating time increases while the nickel loading decrease sharply. Moreover, the content of boron in the Ni−B particles decreases slightly with the Pb^{2+} concentration, consistent with the results of Xin.[18b] Figure 6 shows the high resolution TEM (HRTEM) images of Ni−$B_{3-13.6}$ and Ni−$B_{3-13.6}$(Pb). As anticipated, the flowerlike porous structure of Ni−B particles disappears after the increasing additions of Pb^{2+} in the plating solution. However, the particle sizes of Ni−B particles increase. Figure 6b shows a possible core−shell structure of the Ni−B solid particle. The core (silver) represents the dark background, and the shell (nickel boride) shows amorphous structure. The cause of the solid core−shell particle is mainly because of the change of nickel and boron deposition mechanism at the presence of Pb^{2+} ions. The EDX results of the Ni−$B_{3-13.6}$ and Ni−$B_{3-13.6}$(Pb) show that the nonpresence of Pb element is due to the limitation of testing scope. In addition, the shape of Ni−B particles can be modified

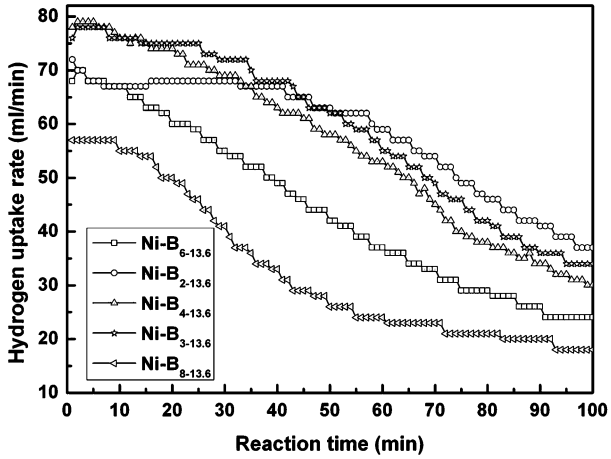

Figure 8. Hydrogen uptake rates over Ni−B catalysts in the hydrogenation of sulfolene. The amount of catalyst in hydrogenation of sulfolene is 0.5 g.

by the addition of a stabilizer. It is desired to add other stabilized metal ions with promoting catalytic properties such as Sn.[31,32]

3.2. Catalytic Properties of Supported Amorphous Ni−B/MgO Catalyst. Figure 7 shows the catalytic sulfolene hydrogenation activity influenced by the pH value. With the increase of the pH value, the catalytic activity increases slightly for all Ni−B_{x-y} series catalysts. The results are attributed to the S_{Ni} value (Table 1). As shown in Figure 2 and Table 1, the S_{Ni} value depends on the load and particles size as well as the composition of Ni−B particles. When the stabilizer was transferred to the EN plating solution, the concentration of nickel decreased sharply due to the change of the structure of Ni−B particles. The results show that the porous structure provides additional active nickel surface. With the disappearance of the porous structure, the conversion of sulfolene descended from 93.1% (Ni−$B_{3-13.6}$, shown in Figure 7) to 17.1% (Ni−$B_{3-13.6}$-3).

To investigate the relation of particle size and the hydrogenation rate,[33] we chose the Ni−$B_{2-13.6}$ (∼25 nm), Ni−$B_{3-13.6}$ (∼35 nm), Ni−$B_{4-13.6}$, (∼41 nm), Ni−$B_{6-13.6}$ (∼45 nm), and Ni−$B_{8-13.6}$ (∼50 nm) with similar nickel loading for the hydrogenation. Table 3 summaries the compositions and activities of as prepared catalysts. Recently, the avid research arises from the drastic increase of the surface to volume ratio to such an extent that the material properties are determined much more by the surface atoms than by the framework atoms with the result that the physical and chemical properties of the nanoparticles differ considerably from those of bulk solids.[34−36] The smaller the particles were, the more surface atoms were prepared. Moreover, Li et al. found that the composition of nickel in Ni−B samples also affects the S_{Ni} value.[37] Thus, the changes of S_{Ni} value should be attributed to the particles sizes and compositions of Ni−B particles. Figure 8 shows the hydrogen uptake rate over different Ni−$B_{x-13.6}$ catalyst during the hydrogenation. Other than Ni−

SCHEME 2: Reaction Scheme of the AP Hydrogenation

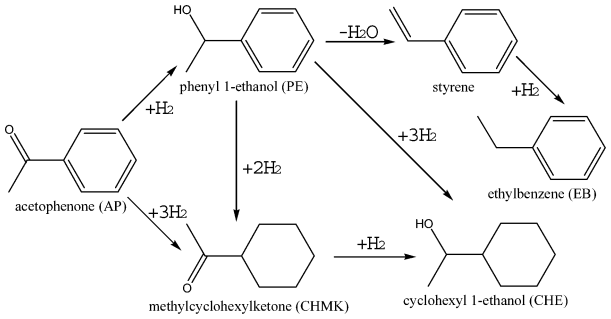

$B_{2-13.6}$, the hydrogen uptake rates depend on the S_{Ni} value, from which the Ni−$B_{3-13.6}$ shows highest initial hydrogen uptake rate. The initial hydrogen uptake rate over Ni−$B_{2-13.6}$ is much smaller than that of Ni−$B_{3-13.6}$ in spite of same S_{Ni} value. The EXAFS (II) program calculation has revealed that the coordination number of Ni decreased with the increase of boron content in Ni−B particles, showing that the Ni active sites became more highly unsaturated at higher B content.[38] Such highly unsaturated Ni active sites may promote the chemisorption of the reactants and, in turn, may increase the hydrogenation activity but reduce the initial hydrogenation rate.[37,39] In our experiment, the decrease of hydrogen uptake rate is slower than the other catalysts, and it may be due to the more highly unsaturated Ni active sites.

For the hydrogenation of sulfolene, the supported Ni−B catalysts from EN plating show excellent activity. It is clear that the hydrogenation rates depend on the surface concentration of nickel, which is affected by particles sizes and composition of Ni−B particles. Besides the sulfolene hydrogenation, the selectivity of catalyst was investigated by hydrogenation of AP, which is important because of the extensive industrial use of the reaction products, 1-phenyl ethanol (PE) and cyclohexyl 1-ethanol (CHE).[39,40] Scheme 2 indicates the reaction route for the hydrogenation AP. Generally, the selectivity of PE and CHE depends on the electronic properties of the catalyst, and the active metal that is rich in electrons prefers to adsorb C═O groups other than aromatic rings, resulting in a higher selectivity for PE production.[41−43] As the Ni atoms accept the electrons from B atoms in nickel boride catalyst,[2,6] the nickel boride catalyst shows poor selectivity of CHE.[44,45] Alternatively, the abundance of electrons around active Ni sites in the supported Ni−B catalyst restrains the absorption of aromatic rings, preventing the hydrogenation of aromatic rings to form methylcyclohexylketone. Moreover, it was observed that at longer reaction times further hydrogenolysis of PE to styrene occurred, leading to the formation of ethylbenzene (EB) in the next hydrogenation, as shown in Figure 9.[46] Figure 9 shows the catalytic activities of AP hydrogenation. In comparison with Ni−$B_{2-13.6}$, Ni−$B_{3-13.6}$, and Ni−$B_{4-13.6}$ catalysts, the conversion of AP over Ni−$B_{2-13.6}$ is the highest. It could be ascribed to the different S_{Ni} values.

On the other hand, the electronic property of supported Ni−B catalyst could affect the selectivity of CHE. From the compositions of Ni−$B_{2-13.6}$, Ni−$B_{3-13.6}$, and Ni−$B_{4-13.6}$ catalysts shown in Table 1, the Ni−$B_{2-13.6}$ catalyst is present with the highest boron content. It should be concluded that the nickel atoms are rich in more electrons, which resulted in decreasing the selectivity of CHE. However, the yield of CHE over these supported Ni−B catalysts varies little from ∼3.7 (Ni−$B_{2-13.6}$) to ∼3.5% (Ni−$B_{4-13.6}$), and the conversion of AP decreases from 97.6 (Ni−$B_{2-13.6}$) to 90.3% (Ni−$B_{4-13.6}$). It suggests that the selectivity of CHE changes slightly from ∼3.8 (Ni−$B_{2-13.6}$) to ∼3.9% (Ni−$B_{4-13.6}$). In our view, rather than the electronic properties of supported Ni−B catalyst, the selectivity of CHE

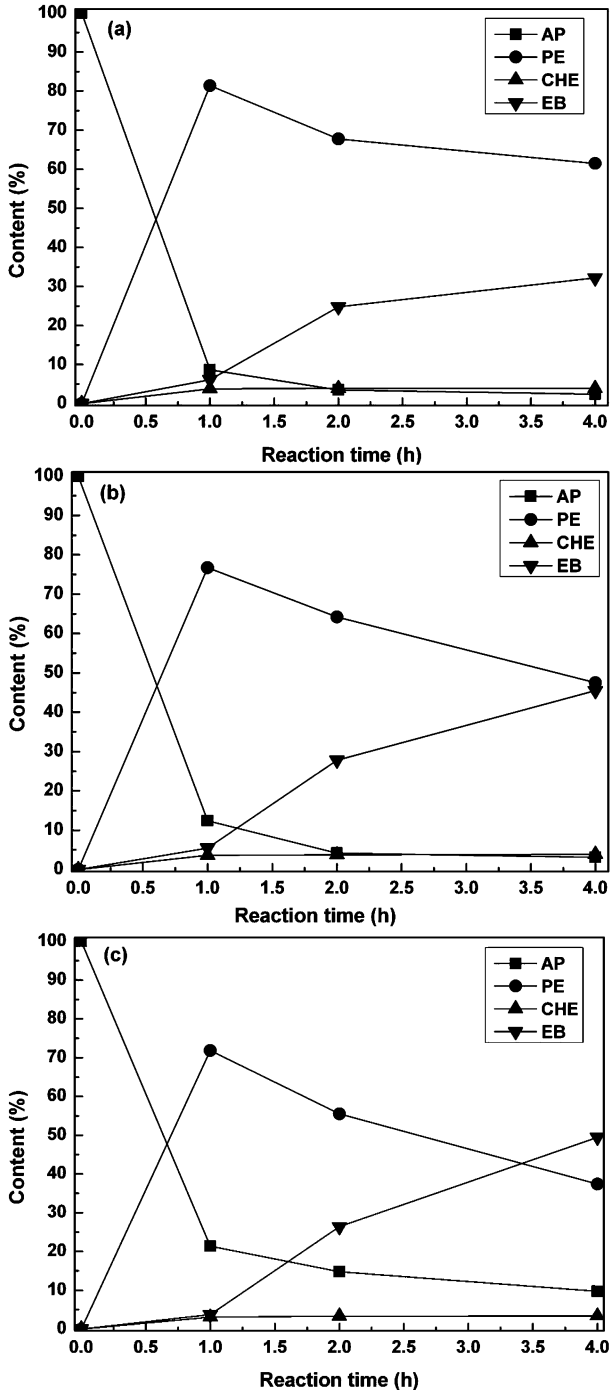

Figure 9. Reaction profiles of AP hydrogenation over (a) the Ni−$B_{2-13.6}$ catalyst, (b) the Ni−$B_{3-13.6}$ catalyst, and (c) the Ni−$B_{4-13.6}$ catalyst.

should also depend on the particle size that is the same as the hydrogenation of cinnamaldehyde.[47,48] For the selectivity of EB over the supported Ni−B catalyst, Figure 9 indicates that the Ni−$B_{2-13.6}$ is present in lowest selectivity. As far as the action of supported alloy/bimetallic catalysts is concerned, the main theories suggest either geometric and/or electronic effects to account for the improved catalytic properties. The geometric or ensemble effects arise due to the dilution of the surface of the given active metal by an inactive one.[49] The ensemble effect can induce different structure sensitivities of the reactions. The Ni−B catalyst can be regarded as a kind of alloy catalyst containing Ni as active metals and B as diluting elements. Scheme 2 shows that the EB comes from the hydrogenolysis of PE to styrene. The dilution of active metal (Ni) surface into

smaller ensembles by addition of inactive species, B, selectively poisons the hydrogenolysis reaction that requires relatively large clusters or ensembles of adjacent metal atoms.[50,51] Therefore, the higher content of boron in the Ni−$B_{2-13.6}$ results in producing less styrene from the hydrogenolysis of AP, which agrees with the result of the EB yields over different supported Ni−B catalysts in Figure 9. In comparison with the Ni−$B_{2-13.6}$, Ni−$B_{3-13.6}$, and Ni−$B_{4-13.6}$, the conversion of AP and content of boron in catalyst is Ni−$B_{2-13.6}$ > Ni−$B_{3-13.6}$ > Ni−$B_{4-13.6}$, while the yield of EB is Ni−$B_{2-13.6}$ < Ni−$B_{3-13.6}$ < Ni−$B_{4-13.6}$. The results show that the higher the content of boron in Ni−B particles was, the lower the selectivity of EB was obtained.

4. Conclusions

We found that the nominal en/Ni^{2+}, pH value, and the stabilizer can affect the size and shape of the Ni−B nanoparticles in different ways. At least under the experimental conditions used in the present work, we can change the sizes and the load of amorphous Ni−B nanoparticles and tune the shape of particle from pores to solid by changing the en/Ni^{2+} molar ratio or pH value and the addition of stabilizer. The results of the sulfolene hydrogenation and acetophenone suggest that the hydrogenation activities depend on the S_{Ni} value, and the selectivity is due to the particle size and composition.

Acknowledgment. The authors are thankful for the financial support of the National Natural Science Foundation of China (Grants 20403009), the Key Project of Chinese Ministry of Education (No. 105045), and Open Foundation of State Key Laboratory of Heavy Oil Processing.

References and Notes

(1) Klabunde, K. J. *Nanoscale Materials in Chemistry*; John Wiley & Sons, Inc.: New York, 2001.

(2) (a) Molnar, A.; Smith, G. V.; Bartok, M. *Adv. Catal.* **1989**, *36*, 329. (b) Wonterghem, J. Van.; Morup, S.; Koch, C. J. W.; Charles, S. W.; Wells, S. *Nature* **1986**, *322*, 622. (c) Chen, Y. *Catal. Today* **1998**, *44*, 3. (d) Deng, J. F.; Li, H. X.; Wang, W. J. *Catal. Today* **1999**, *51*, 113. (e) Ganem, B; Osby, J. O. *Chem. Rev.* **1986**, *86*, 763.

(3) Skrabalak, S. E.; Suslik, K. S. *Chem. Mater.* **2006**, *18*, 3103.

(4) (a) Glavee, G. N.; Klabunde, K. J.; Sorensen, C. M.; Hadjipanayis, G. C. *Langmuir* **1992**, *8*, 771. (b) Glavee, G. N.; Klabunde, K. J.; Sorensen, C. M.; Hadjipanayis, G. C. *Langmuir* **1993**, *9*, 162. (c) Glavee, G. N.; Klabunde, K. J.; Sorensen, C. M.; Hadjipanayis, G. C. *Langmuir* **1994**, *10*, 4726. (d) Glavee, G. N.; Klabunde, K. J.; Sorensen, C. M.; Hadjipanayis, G. C. *Inorg. Chem.* **1993**, *32*, 474. (e) Glavee, G. N.; Klabunde, K. J.; Sorensen, C. M.; Hadjipanayis, G. C. *Inorg. Chem.* **1995**, *34*, 28.

(5) (a) Brown, H. C.; Brown, C. A. *J. Am. Chem. Soc.* **1963**, *85*, 1005. (b) Brown, C. A. *J. Org. Chem.* **1970**, *35*, 1900. (c) Brown, C. A.; Ahuja, V. K. *J. Org. Chem.* **1973**, *38*, 2226. (d) Paul, R.; Buisson, P.; Joseph, N. *Ind. Eng. Chem.* **1952**, *44*, 1006.

(6) Min, E. Z.; Li, C. Y. *Base of Science and Engineering of Green Petrochemical Technology*; Chinese Petrochem Press: Beijing, 2002.

(7) Davis, S. C.; Klabunde, K. J. *Chem. Rev.* **1982**, *82*, 153.

(8) (a) Armadi, T. S.; Wang, Z. L.; Green, T. C.; Heinglein, A.; El-Sayed, M. A. *Science* **1996**, *272*, 1924. (b) Tautster, S. J.; Fung, S. C. *J. Catal.* **1978**, *5*, 29. (c) Mustard, D. G.; Bartholomew, C. H. *J. Catal.* **1981**, *67*, 186. (d) Zelinski, J. *J. Catal.* **1982**, *76*, 157. (e) Molina, R.; Poncelet, G. *J. Catal.* **1998**, *173*, 257. (f) Boudjahem, A. G.; Monteverdi, S.; Mercy, M.; Bettahar, M. M. *J. Catal.* **2004**, *221*, 325.

(9) (a) Ferri, D.; Mondelli, C.; Krumeich, F.; Baiker, A. *J. Phys. Chem. B* **2006**, *110*, 22982. (b) Zheng, N. F.; Stucky, G. D. *J. Am. Chem. Soc.* **2006**, *48*, 14278. (c) Liu, Z. P.; Wang, C. M.; Fan, K. N. *Angew. Chem. Int. Ed.* **2006**, *41*, 6865.

(10) (a) Meiwes-Broer, K. H. *Cluster-Solid Surface Interaction*; Springer: Berlin, 1999. (b) Heiz, U.; Sanchez, A.; Abbet, S.; Schneider, W. D. *J. Am. Chem. Soc.* **1999**, *121*, 3214.

(11) (a) Miyazaki, A.; Balin, I.; Aika, K.; Nakano, Y. *J. Catal.* **2001**, *204*, 364. (b) Reinen, D.; Selwood, P. W. *J. Catal.* **1963**, *2*, 109. (c) Houalla, M.; Lemaître, J.; Delmon, B. *J. Chem. Soc., Faraday Trans.* **1982**, *78*, 1389. (d) Gavallas, G. R.; Phishitkul, C.; Voecks, G. E. *J. Catal.* **1984**, *88*, 54.

(12) (a) Chen, X. Y.; Wang, S.; Zhuang, J. H.; Qiao, M. H.; Fan, K. N.; He, H. Y. *J. Catal.* **2004**, *227*, 419. (b) Chen, X. Y.; Hu, H. R.; Liu, B.; Qiao, M. H.; Fan, K. N.; He, H. Y. *J. Catal.* **2003**, *220*, 254. (c) Li, H. X.; Zhao, Q. F.; Wan, Y.; Dai, W. L.; Qiao, M. H. *J. Catal.* **2006**, *244*, 251.

(13) Xie, S. H.; Qiao, M. H.; Zhou, W. Z. *J. Phys. Chem. B* **2005**, *109*, 24361.

(14) (a) Lewis, L. N. *Chem. Rev.* **1993**, *93*, 2693. (b) Gates, B. C. *Chem. Rev.* **1995**, *95*, 511.

(15) Lu, P.; Teranishi, T.; Asakura, K.; Miyake, M.; Toshima, N. *J. Phys. Chem. B* **1999**, *103*, 9673.

(16) (a) Xue, D.; Deng, J. F. *Mater. Lett.* **2001**, *47*, 271. (b) Chen, X. Y.; Yang, W. L.; Wang, S.; Qiao, M. H.; Yan, S. R.; Fan, K. N.; He, H. Y. *New J. Chem.* **2005**, *29*, 266. (c) Tierno, P.; Goedel, W. A. *J. Phys. Chem. B* **2006**, *110*, 3043.

(17) Mallory, G. O.; Hajdu, J. B. *Electroless Plating: Fundamentals and Applications*; American Electroplaters and Surface Finishers Society: Orlando, FL, 1990.

(18) (a) Lee, L.; Hammond, P. T.; Rubner, M. F. *Chem. Mater.* **2003**, *15*, 4586. (b) Yin, X.; Hong, L.; Chen, B. H.; Ko, T. M. *J. Colloid Inter. Sci.* **2003**, *262*, 89. (c) Yin, X.; Hong, L.; Chen, B. H. *J. Phys. Chem. B* **2004**, *108*, 10919. (d) Chen, C. H.; Chen, B. H.; Hong, L. *Chem. Mater* **2006**, *18*, 2959.

(19) (a) Wu, Z. J.; Zhang, M. H.; Ge, S. H.; Zhang, Z. L.; Li, W.; Tao, K. Y. *J. Mater. Chem.* **2005**, *15*, 4928. (b) Ge, S. H.; Wu, Z. J.; Zhang, M. H.; Li, W.; Tao, K. Y. *Ind. Eng. Chem. Res.* **2006**, *45*, 2229.

(20) Yin, Y. D.; Li, Z. Y.; Zhong, Z. Y.; Gates, B.; Xia, Y. N.; Venkateswaran, S. *J. Mater. Chem.* **2002**, *12*, 522.

(21) (a) Li, H. X.; Li, H.; Dai, W. L.; Qiao, M. H. *Appl. Catal. A* **2003**, *238*, 119. (b) Wang, W. J.; Qiao, M. H.; Yang, J.; Xie, S. H.; Deng, J. F. *Appl. Catal. A* **1997**, *163*, 101. (c) Klvana, D.; Chaouki, J.; Kusohorsky, D.; Chavarie, C.; Pajonk, G. M. *Appl. Catal. A* **1988**, *42*, 121. (d) Bartholomew, C. W.; Farrauto, R. J. *J. Catal.* **1976**, *45*, 41.

(22) Roucoux, A.; Schulz, J.; Patin, H. *Chem. Rev.* **2002**, *102*, 3757.

(23) Riedel, W. *Electroless Nickel Plating*; ASM International, Finishing Publications: Metal Park, OH, 1991.

(24) Jiang, X. X.; Shen, W. *The Fundamental and Practice of Electroless Plating*; National Defence Ind Press: Beijing, 2000.

(25) Agarwala, R. C.; Agarwala, V. *Sadhana* **2003**, *28*, 475.

(26) Brunelle, J. P. *Pure Appl. Chem.* **1978**, *50*, 1211.

(27) (a) Boudjahem, A. G.; Monteverdi, S.; Mercy, M.; Mettahar, M. M. *Langmuir* **2004**, *20*, 208. (b) Boudjahem, A. G.; Monteverdi, S.; Mercy, M.; Mettahar, M. M. *J. Catal.* **2004**, *221*, 325.

(28) (a) Wu, W. H.; Xu, J. *Catal. Commun.* **2004**, *5*, 591. (b) Wu, W. H.; Xu, J. *Appl. Catal. B* **2005**, *60*, 129.

(29) Greer, A. L. *Acta. Metal. Mater.* **1982**, *30*, 171.

(30) Li, H.; Li, H. X.; Deng, J. F. *Mater. Lett.* **2001**, *50*, 41.

(31) Charbonnier, M.; Romand, M. *Int. J. Adhes. Adhes.* **2003**, *23*, 277.

(32) (a) Wang, Y. Z.; Qiao, M. H.; Hu, H. R.; Yan, S. R.; Wang, W. J.; Fan, K. N. *Acta Chim. Sin.* **2004**, *62*, 1349. (b) Pei, Y.; Hu, H. R.; Fang, J.; Qiao, M. H.; Dai, W. L.; Fan, K. N.; Li, H. X. *J. Mol. Catal., A* **2004**, *211*, 243.

(33) Rampino, L. D.; Nord, F. F. *J. Am. Chem. Soc.* **1942**, *63*, 2745.

(34) Halperin, W. P. *Rev. Mod. Phys.* **1998**, *58*, 533.

(35) Schmid, G. *Chem. Rev.* **1992**, *92*, 1709.

(36) Volokin, Y.; Sinzig, J.; De Jong, L. J.; Schmid, G.; Vargaftik, M. N.; Moisseev, I. I. *Nature* **1996**, *384*, 624.

(37) Li, H. X.; Li, H.; Dai, W. L.; Qiao, M. H. *Appl. Catal. A* **2003**, *238*, 119.

(38) Chen, J.; Lu, G.; Ma, L. *J. Fudan Univ., Nat. Sci.* **1989**, *28*, 78.

(39) Del Angel, G.; Benitez, J. L. *J. Mol. Catal.* **1994**, *94*, 409.

(40) Rajashekharam, M. V.; Bergult, I.; Fouilloux, P.; Schweich, D.; Delmas, H.; Chaudhari, R. V. *Catal. Today* **1999**, *48*, 83.

(41) Koscielski, T.; Bonnier, J. M.; Damon, J. P.; Masson, J. *Appl. Catal.* **1989**, *49*, 91.

(42) Lin, S. D.; Sanders, D. K.; Vannice, M. A. *J. Catal.* **1994**, *147*, 370.

(43) Masson, J.; Vidal, S.; Cividino, P.; Fouilloux, P.; Court, J. *Appl. Catal.* **1993**, *99*, 147.

(44) Wang, Y. Z.; Qiao, M. H.; Hu, H. R.; Yan, S. R.; Wang, W. J.; Fan, K. N. *Acta Chim. Sin.* **2004**, *62*, 1349.

(45) Sheng, C.; Zhou, S. Y.; Li, H. X. *Acta Phys-Chim. Sin.* **1998**, *14*, 164.

(46) Malyala, R. V.; Rode, C. V.; Arai, M.; Hegde, S. G.; Chaudhari, R. V. *Appl. Catal. A* **2000**, *193*, 71.

(47) Giroir-Fendler, A.; Richard, D.; Ggllezot, P. *Catal. Lett.* **1990**, *5*, 175.

(48) Li, H. X.; Chen, X. F.; Wang, M. H.; Xu, Y. P. *Appl. Catal. A* **2002**, *225*, 117.

(49) (a) Dowden, D. A. In *Proceedings of the 6th International Congress on Catalysis*; Bond, G. C., Wells, P. B., Tompkins, F. C., Eds.; The Chemical Society: London, 1976: vol. 1, pp 621−631. (b) Ponec, V.; Sachtler, W. M. H. In *Proceedings of the 6th International Congress on Catalysis*; Bond, G. C., Wells, P. B., Tompkins, F. C., Eds. The Chemical Society: London, 1976; vol. 1, pp 645−652.

(50) Biloen, P.; Dautzenberg, F. M.; Sachtler, W. M. H. *J. Catal.* **1977**, *50*, 77.

(51) Coq, B.; Figueras, F. *J. Catal.* **1984**, *85*, 197.